ORIGINAL PAPER

Three-dimensional finite element analysis on cochlear implantation electrode insertion

Liu-Jie Ren[1] · Yi Yu[2] · Yu-Heng Zhang[3] · Xin-Dong Liu[3] · Zeng-Jun Sun[3] · Wen-Juan Yao[4] · Tian-Yu Zhang[1] · Cheng Wang[3] · Chen-Long Li[1]

Abstract

Studying the insertion process of cochlear implant (CI) electrode array (EA) is important to ensure successful, sufficient, and safe implantation. A three-dimensional finite element (FE) model was developed to simulate the insertion process. The cochlear structures were reconstructed from an average statistical shape model (SSM) of human cochlea. The electrode is simplified as a long and tapered beam of homogeneous elastic materials, contacting and interacting with the stiff cochlear structures. A quasi-static insertion simulation was conducted, the insertion force and the contact pressure between the electrode and the cochlear wall, were calculated to evaluate the smoothness of insertion and the risk of potential cochlear trauma. Based on this model, different EA designs were analyzed, including the Young's modulus, the straight or bended shape, the normal or a more tapped section size. The influence of the insertion angle was also discussed. Our simulations indicate that reducing the EA Young's modulus, tapering and pre-bending are effective ways to ensure safe and successful EA implantation. This model is beneficial for optimizing EA designs and is potentially useful for designing patient-specific CI surgery.

Keywords Cochlear implant · Electrode array · Finite element · Insertion force · Contact pressure

Liu-Jie Ren and Yi Yu have equally contributed to this work.

✉ Cheng Wang
wangc@shlst.com.cn

✉ Chen-Long Li
chenlong.li@hotmail.com

Liu-Jie Ren
renliujie@fudan.edu.cn

Yi Yu
2200009@sumhs.edu.cn

1 Department of Facial Plastic Reconstructive Surgery, ENT Institute, Eye and ENT Hospital, NHC Key Laboratory of Hearing Medicine (Fudan University), Shanghai 200031, China

2 School of Medical Instrumentation, Shanghai University of Medicine and Health Sciences, Shanghai 201318, China

3 Shanghai Engineering Research Center of Cochlear Implants, Shanghai 201318, China

4 School of Mechanics and Engineering Science, Shanghai Institute of Applied Mathematics and Mechanics, Shanghai University, Shanghai 200444, China

1 Introduction

Cochlear implant (CI) provides significant benefit to patients with severe to profound sensorineural hearing loss due to diseases or aging (Zeng et al. 2008). It bypasses the acoustic hearing pathway by directly stimulate the auditory nerves in the cochlea, which is the most important hearing organ. CI consists of the outside wearable audio processor and the surgically implanted component. The audio processor transmits sounds into electric signals, and transfers the signal to the implanted part via a pair of RF coils. Then the signal stimulates the cochlear nerves via an electrode array (EA), which is inserted into the cochlea.

Clinical evidences have proven that the EA insertion process during the CI surgery is crucial for patients outcomes (Holden et al. 2013). The EA may damage soft cochlear tissues including the hearing organs during the insertion, causing further damage to the residual hearing of the patients, and influence the electric-acoustic stimulation (Roland and Wright 2006). Furthermore, the intracochlear trauma may also increasing the risk of fibrosis and ossification (Fayad et al. 2009). Studies in healthy human temporal bones (De Seta et al. 2017) and postmortem CI-implanted

patients (Kamakura and Nadol 2016) have shown trauma in the ligament and basilar membrane, which bears the hearing cells and nerves. Great efforts have been done to avoid or minimize the insertion-induced trauma, including optimization of both the EA designs and the surgical inserting procedure (Risi 2018, Grayeli et al. 2014). Technologies of using robot-aided EA implantation are also developed to ensure a smooth and safe insertion (Majdani et al. 2009; Caversaccio et al. 2017).

Influencing factors to minimize the trauma includes the insertion angle, the speed and most importantly, the structural and mechanical properties of the designed EA (Rajan et al. 2013; Aebischer et al. 2021; Chen et al. 2003). These factors affect the insertion dynamics greatly. Although the configuration of an inserted EA were observed using various techniques (CT of different resolutions, postmortem sectioning, etc.), in vivo observation of the EA insertion process is very difficult. Moreover, the interaction between the EA and the cochlear structures is invisible due to limitation of current imaging technologies. A successful EA insertion should be sufficient, smooth and safe, the contact force of the electrode tip is essential but difficult to measure (Wade et al. 2014).

To obtain comprehensive understanding of the EA insertion process, finite element analysis (FEA) have been adopted (Chen et al. 2003; Lim et al. 2005; Kha et al. 2007; Kha and Chen 2012; Goury et al. 2016; Areias et al. 2021). The advantage of FEA is twofolds. Firstly, the cochlear and EA models are uniform, allowing an exact univariate analysis, while experimental studies are interfered by individual geometrical differences between specimens, and also by variations of mechanical properties among different manufactured EAs. Secondly, FEA transparentize the dynamic insertion process, allowing to obtain forces and pressures that are difficult or impossible to obtain during surgeries or experiments.

An early simplified 2D EA insertion model was developed by Chen et al. (2003), the bulking and tip contact pressure of different EA designs were studied. Later, they developed a 3D model and evaluated the trauma via contact frequency and shear stress near the electrode tip (Kha et al. 2007; Kha and Chen 2012). Goury et al. (2016) developed a 3D FEA model to simulate the EA insertion process, they found that the insertion angle is a parameter related with insertion failure (Goury et al. 2016). A recent 3D model was developed by Areias et al. (2021), the insertion process was fully simulated and mechanical properties of different EA designs was discussed. Furthermore, FEA models were also developed to simulate the electrical stimulations of EAs (Kalkman et al. 2016), and there also exists non-physical algorithms for fast prediction of the implanted configuration of EAs (Duchateau et al. 2015).

In this paper, we proposed a 3D finite element model to simulate the complete insertion process of the EA. Four types of EA were created (by tapering the section size or pre-bending the EA) and simulated, the insertion force and tip contact pressure were calculated, and then the influences of tapering and pre-bending were discussed. Other factors were also investigated, including the stiffness of the EAs and the inserting angles. This model is beneficial to the design of EA as well as to further computer-aided patient-specific designs of CI surgery.

2 Modeling

2.1 Cochlea model—geometry and mesh

Cochlea is a long, spiral tube filled with lymph, separated into three chambers (scala vestibula, scala media and scala tympani) by two membranes (the Reissner's membrane and the basilar membrane). The cochlear walls are mostly dense bony structures. The EA is inserted into the scala tympani, either through the round window at the base of the cochlea, or through an artificially drilled hole near the round window. Therefore, for a convincible simulation of the CI insertion, an proper geometrical reconstruction of the cochlear walls, especially the scala tympani is essential. The geometry of cochlea walls can be generated using either simplified semi-analytically described shapes (Lim et al. 2005), or from CT reconstructions (Kha and Chen 2012; Goury et al. 2016; Areias et al. 2021). However, semi-analytical simplifications seems to lose many detailed features, while CT reconstruction may bring in information that are individually dependent, due to the variation of cochlea. In this paper, we adopted the "average cochlea" of more than 100 cochlear samples (including both males and females). The open-source average cochlea was built up using the statistical shape model (SSM) and shared by Gerber et al. (2017). It has been reported that the cochlear length has significant differences between males and females but not related with age (Sato et al. 1991). Moreover, slight differences have also been reported between ethnic groups (Thong et al. 2017). Therefore, although the usage of our average cochlea model may lose some gender related details, but would be able to give a general knowledge of the EA insertion process.

The SSM of cochlea was originally represented by a series of about 95,259 points or landmarks in 3D space, forming a point cloud (see Fig. 1A)[1] To generate a finite element mesh of the model, following procedures were performed. Firstly, surface reconstruction using the ball

---

[1] The SSM model is shared at SICAS Medical Image Repository, https://doi.org/10.22016/smir.o.207473, with CC-BY 3.0 license.
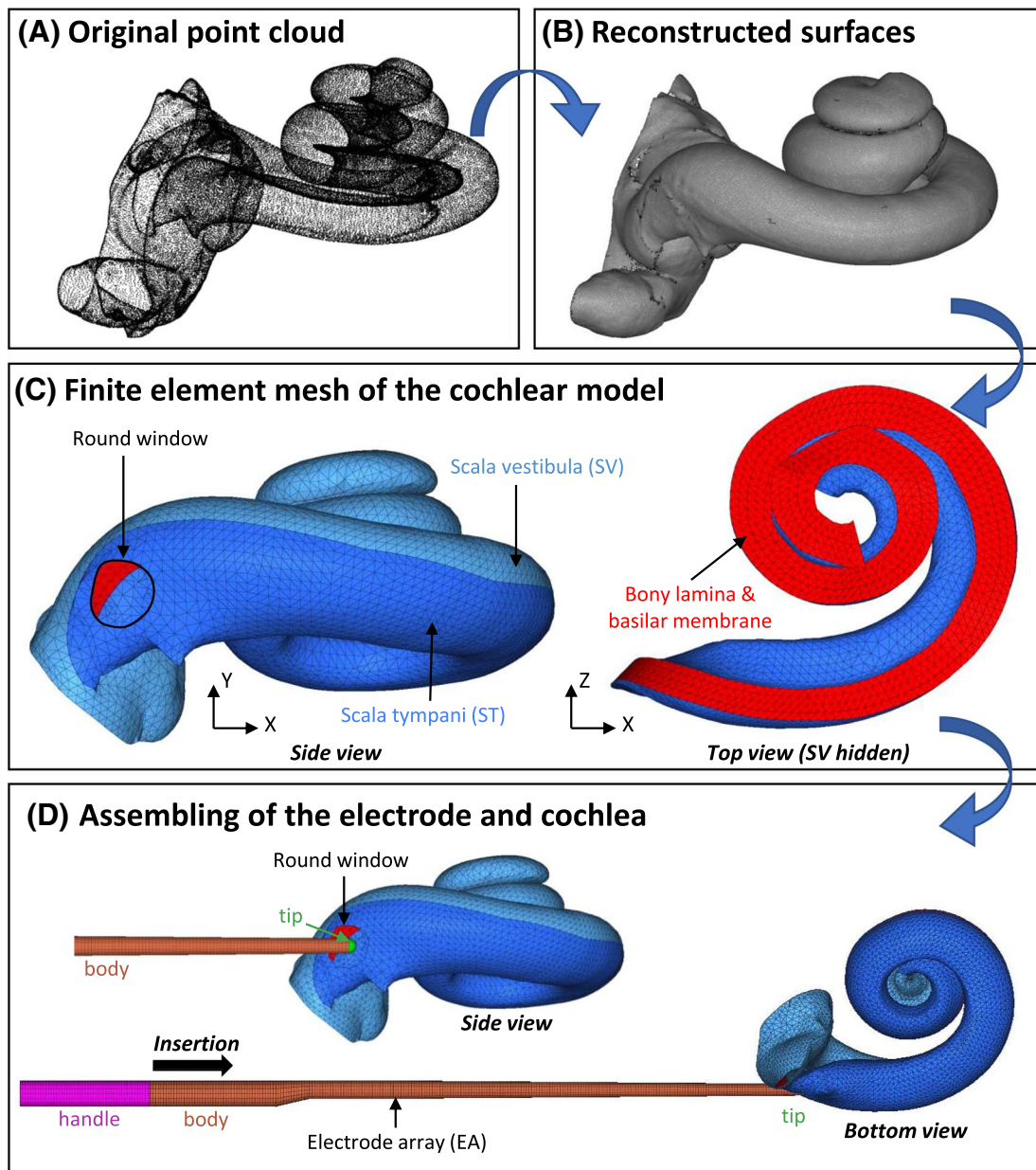
(A) Original point cloud

(B) Reconstructed surfaces

(C) Finite element mesh of the cochlear model

Round window

Scala vestibula (SV)

Bony lamina & basilar membrane

Scala tympani (ST)

Side view

Top view (SV hidden)

(D) Assembling of the electrode and cochlea

Round window

tip

body

Side view

Insertion

handle body

Electrode array (EA)

tip

Bottom view

Fig. 1 The finite element cochlear model. **A** Original point cloud; **B** Reconstructed surfaces, with a few geometrical errors; **C** Finite element mesh of the cochlea, consisting of the scala vestibula, the scala tympani, bone lamina and the basilar membrane. The height of the cochlea is about 3.5 mm (in Y-direction) and the width is about 7.5 mm (in Z-direction); **D** Assembling of the cochlea and electrode model. The tip of electrode array locates at the center of the round window

pivoting algorithm was conducted within the open-source geometry processing software MeshLab (v1.3.0b). The reconstructed surfaces, described by triangular patches, had quite a few geometrical errors (see Fig. 1B). Moreover, the triangular patches were irregular and of poor-quality so that the model could not be directly used for an FEA simulation. Therefore, the second step was to manually correct those geometrical errors with the finite element preprocessor HyperMesh (v14.0, Altair). Meanwhile, the model was

re-meshed with regular and uniform meshes. Since the re-meshed model lacks the basilar membrane and bony lamina that separate the cochlea, these lacked structures were generated according to geometrical characteristics of the cochlear walls (see Fig. 1C, top view). Besides, a roughly round hole was made at the base of the cochlear model, representing the round window for EA insertion.

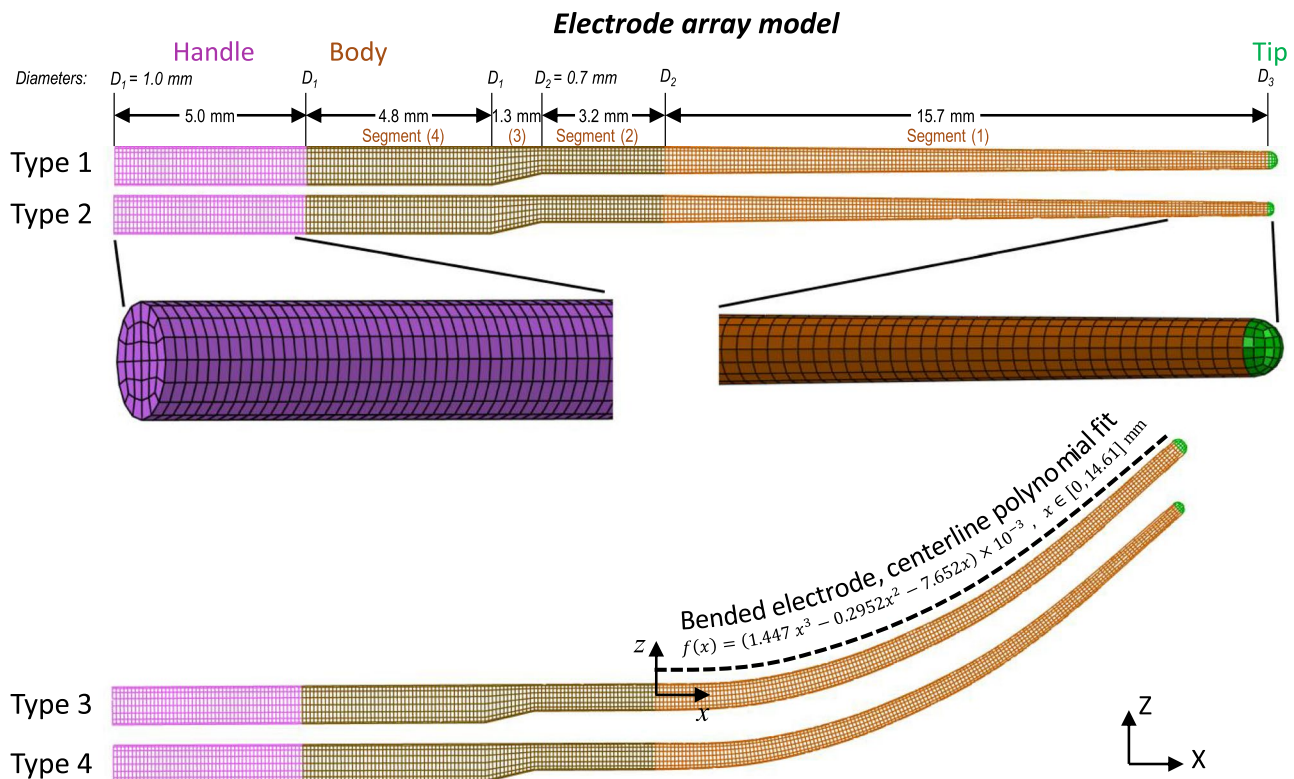Since the bony walls were much stiffer (about several GPa) than the EA, the cochlear walls were meshed with

Fig. 2 The model of electrode array. Four types with different geometrical parameters are presented. Type 1 - straight electrode with normal tapered section size; type 2 - straight electrode with more tapered (or softened) section size; type 3, bended electrode with normal section, and type 4 - bended and softened electrode

3-node triangular shell elements and modeled as rigid body, with all translational and rotations degrees of freedom (DOF) constrained. The cochlear model had 7,517 nodes and 15,294 elements (see Fig. 1C). Figure 1D shows the assembling of the cochlear model and the EA model, which will be discussed later.

2.2 EA and contact modeling

The EA model is a simplification of the commercial EA (LCI-20PI, Listent, China), which is designed to be inserted along the lateral wall of the cochlea. The geometrical and material data were provided by Hearing Medicine Key Laboratory, National Health Commission of China. The EA is composed with metal electrodes immersed in the silicon base. In our model, the EA was described as a uniform material, which is a common simplification. The simplified EA consisted of the handle, the body, and the tip. The handle was a cylinder, the tip was a semi-sphere, and the body consisted of four segments, (1) a tapered cylinder (length, 15.7 mm; diameter ranges linearly from $D_2 = 0.7$ mm to D_3), (2) a cylinder segment (length, 3.2 mm; diameter $D_2 = 0.7$ mm), (3) a connecting segment (length 1.3 mm, diameter changes from $D_1 = 1.0$ mm to $D_2 = 0.7$mm), and (4) another

cylinder segment (length, 4.8 mm; diameter $D_1 = 1.0$ mm), see Fig. 2. The insertion depth of the designed EA is about 20.2~25.0 mm in practice. For a full-length implantation, an enlargement of the round window may be needed, since the diameter of the round window is about 1.0 mm. For some patients with smaller round window size or cochlear size, an alternative is to only implant segments (1) to (3). In our simulation, a fully implantation process was simulated.

In this study, we compared the straight and pre-bended EA, and also compared the normal shape and a softened tapered shape (fulfilled by further tapering the EA), making four different combinations for the EA, we named them type 1 (straight, normal), 2 (straight, tapered), 3 (bended, normal) and 4 (bended, tapered), respectively, see Fig. 2. The geometrical parameters of the normal and tapered EA are listed in Table 1. The tapered EA has a smaller diameter near the tip, thus being more soft. The bended EA has the same geometrical parameters as the straight one, except for a bended central axis line, which was approximated by a polynomial function. The EA body and handle are longitudinally divided into 300 divisions (250 divisions for the body and 50 divisions for the handle), and meshed with structured block elements. Abaqus C3D8R elements were used, the EA model contained 12,432 nodes and 9,680 elements in total.

Table 1 Geometrical parameters of the electrode array

Electrode part	Geometrical parameters	Values and descriptions
Handle	Length	5.0 mm
	Diameter	1.0 mm
Body - segment (1)	Length	15.7 mm
	Diameter	Linearly tapered $D_2 \sim D_3$ 0.7~0.45 mm (normal, type 1,3) 0.7~0.35 mm (softened, type 2,4)
Body - segment (2)	Length	3.2 mm
	Diameter	$D_2 = 0.7$ mm
Body - segment (3)	Length	1.3 mm
	Diameter	Linearly tapered, $D_1 \sim D_2$ 1.0~0.7 mm
Body - segment (4)	Length	4.8 mm
	Diameter	$D_1 = 1.0$ mm
Tip	Radius	$D_3/2$ 0.225 mm (normal, type 1,3) 0.175 mm (softened, type 2,4)

The Young's modulus of EA is the most important parameter (Kha et al. 2004), adopted to be several hundreds MPa in previous models, dependent on different electrodes. The effective Young's modulus of our EA is about 300 MPa. Therefore, we chose three values (150 MPa, 300 MPa and 600 MPa) for parameter analysis. The Poisson ratio of electrodes are chosen to be 0.3. The density of EA is around 1.5 kg/m^3. Since the insertion of EA is a very slow process, the mass effect is ignorable and the density is insensitive.

The node-to-surface contact algorithm is adopted to mimic the interaction between the electrode and the cochlea walls, and fulfilled in Abaqus. A full contact definition includes the normal and tangent behavior. For the normal behavior, the "hard contact" assumption was used; for the tangent behavior, the Coulomb friction model was obtained. The influence of the friction coefficient has been reported an influencing factor (but hard to determine) to the inserting process, an evaluation of 0.1 was adopted according to literature data (Areias et al. 2021; Kha and Chen 2006).

2.3 EA insertion simulation

The EA insertion process is simulated in the time domain. The dynamics of EA should satisfy that

$$\mathbf{M} \cdot \ddot{u} + \mathbf{K} \cdot u = f^{\text{insertion}} + f^{\text{contact}} \qquad (1)$$

where u is the displacement of EA nodes (including x, y and z components) and f is the acting force to the EA due to insertion or contact, $\mathbf{M}$ and $\mathbf{K}$ are the assembled mass and stiffness matrices, respectively. A quasi-statistic simulation was adopted, thus the mass matrix is virtually scaled to solve the equilibrium equation

$$\mathbf{K} \cdot u = f^{\text{insertion}} + f^{\text{contact}} \qquad (2)$$

The insertion process was divided into multiple sub-steps, ensuring a smooth implantation. At the beginning of the insertion, the straight EA was set in place, with its tip located at the center of the round window. Then the EA was inserted by a total of 250 sub-steps (corresponding to the mesh divisions of the EA body, each sub-step corresponds to 0.1 mm insertion). For each sub-step, to mimic a small insertion, a displacement boundary condition to the nodes that are out of the cochlea were given; and the displacement of the nodes in the cochlea were calculated by solving the equilibrium equation. Since the contact pressure and insertion force were strongly related to the deformation of the EA, an iterative process was necessary to solve the nonlinear problem. To inserting the bended EA, an initial straighten step was added. This would create stress within the EA, which would be gradually released during the step-by-step insertion process. Due to the larger diameter of segment (4) of EA body ($D_1 = 1$mm), when the insertion depth exceeds about 20 mm, the insertion simulation may fail due to overlap between the EA body and the round window. Therefore, to ensure successful insertion, the contact between segment (4) of the EA body and the cochlear base were suppressed, mimicking an enlargement of the round window.

2.4 Simulation and data processing

All the simulations were conducted in Abaqus (v6.13, Dassault Systems), with a desktop computer (CPU 2.70GHz, 16 GB RAM, Window 10 system). The simulation results were extracted using Abaqus Python Interface, and further analyzed with MATLAB (R2020a, Mathworks).
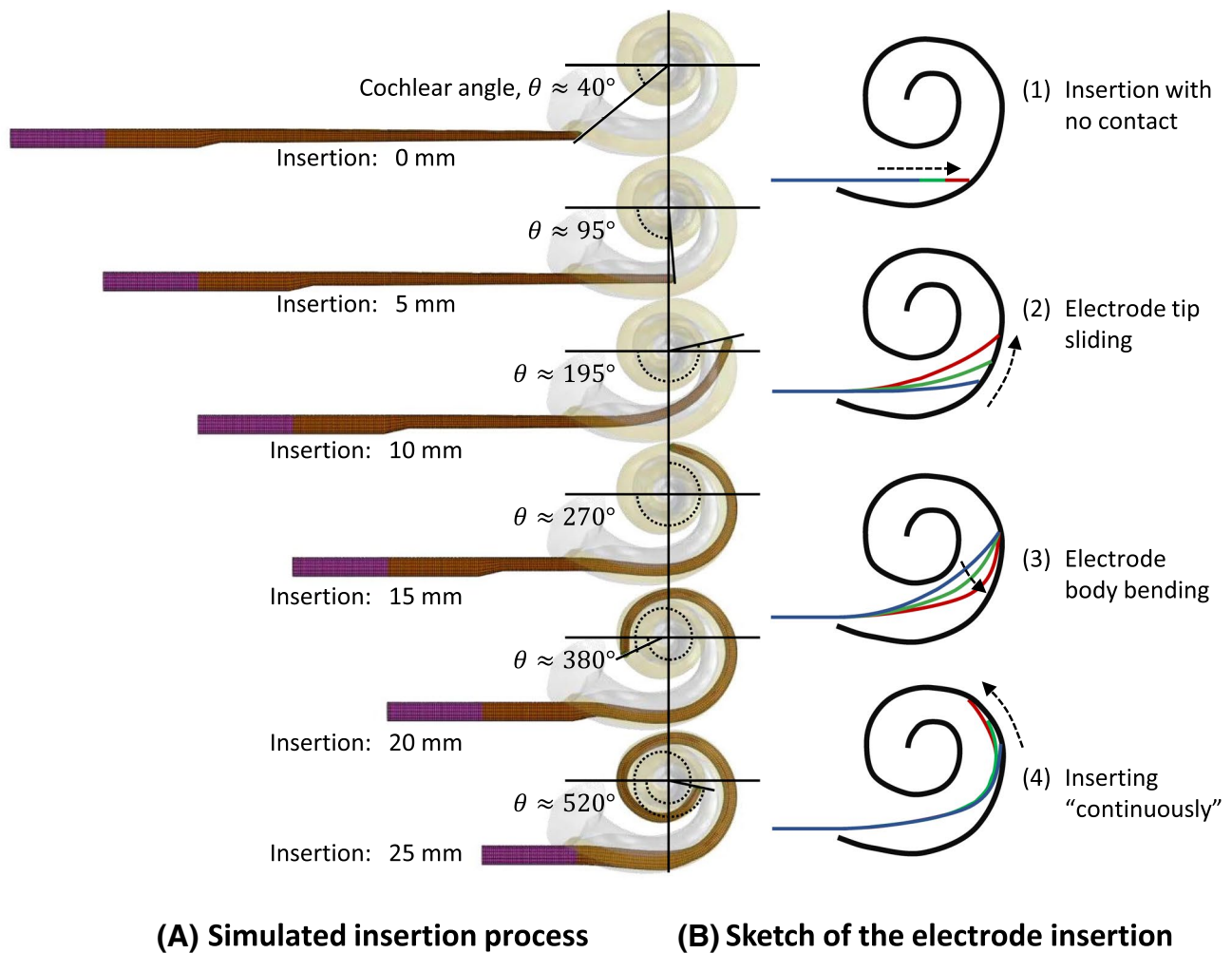
(A) Simulated insertion process   **(B) Sketch of the electrode insertion**

Fig. 3 The electrode insertion process. **A** The simulated insertion results (electrode type 1, 300 MPa, friction ratio 0.1), snaps of insertion depth 0, 5, 10, 15, 20, and 25 mm, with corresponding cochlear angles $\theta = 40°, 95°, 195°, 270°, 380°$ and $520°$; (B) 2D sketches of the insertion process. Four different stages occur during the insertion process

3 Results and discussion

3.1 The EA inserting process

Figure 3 gives the simulated inserting process of the type 1 electrode (assuming Young's modulus 300 MPa, friction coefficient 0.1) for demonstration purpose. Configurations of the EA are shown at five different insertion depth, 0 mm, 5 mm, 10 mm, 15 mm, 20 mm and 25 mm. As shown in the corresponding 2D sketches, the insertion process can be divided into the following procedures: (1) Non-contact insertion when the EA does contact the cochlea wall, (2) the EA tip contacts and slides along the cochlear lateral wall, (3) the EA bends toward the lateral wall of the cochlea, (4) the EA fully contacts with the cochlear walls for further "continuous" insertion to its full length. Note that the process (2) and (3) may appear repeatedly. Besides the insertion depth,

the electrode tip location may alternatively be evaluated using the cochlea angle, θ (Xu et al. 2000). In this simulation, when the 25 mm electrode was fully implanted, the cochlear angle is about 520°. During the whole insertion process, the EA tip slides along the lateral wall of the cochlea, therefore, the trauma to the structures of the lateral wall is the most commonly reported (Roland and Wright 2006).

3.2 Influence of the EA stiffness on insertion force and contact pressure

The contact force / pressure between the EA and cochlear wall is an essential fact related to cochlea damage. Although difficult to measure during the cochlear implantation surgeries or experiments, the contact force / pressure is feasible to obtain using numerical simulations. Meanwhile, the insertion force is another essential parameter to evaluate
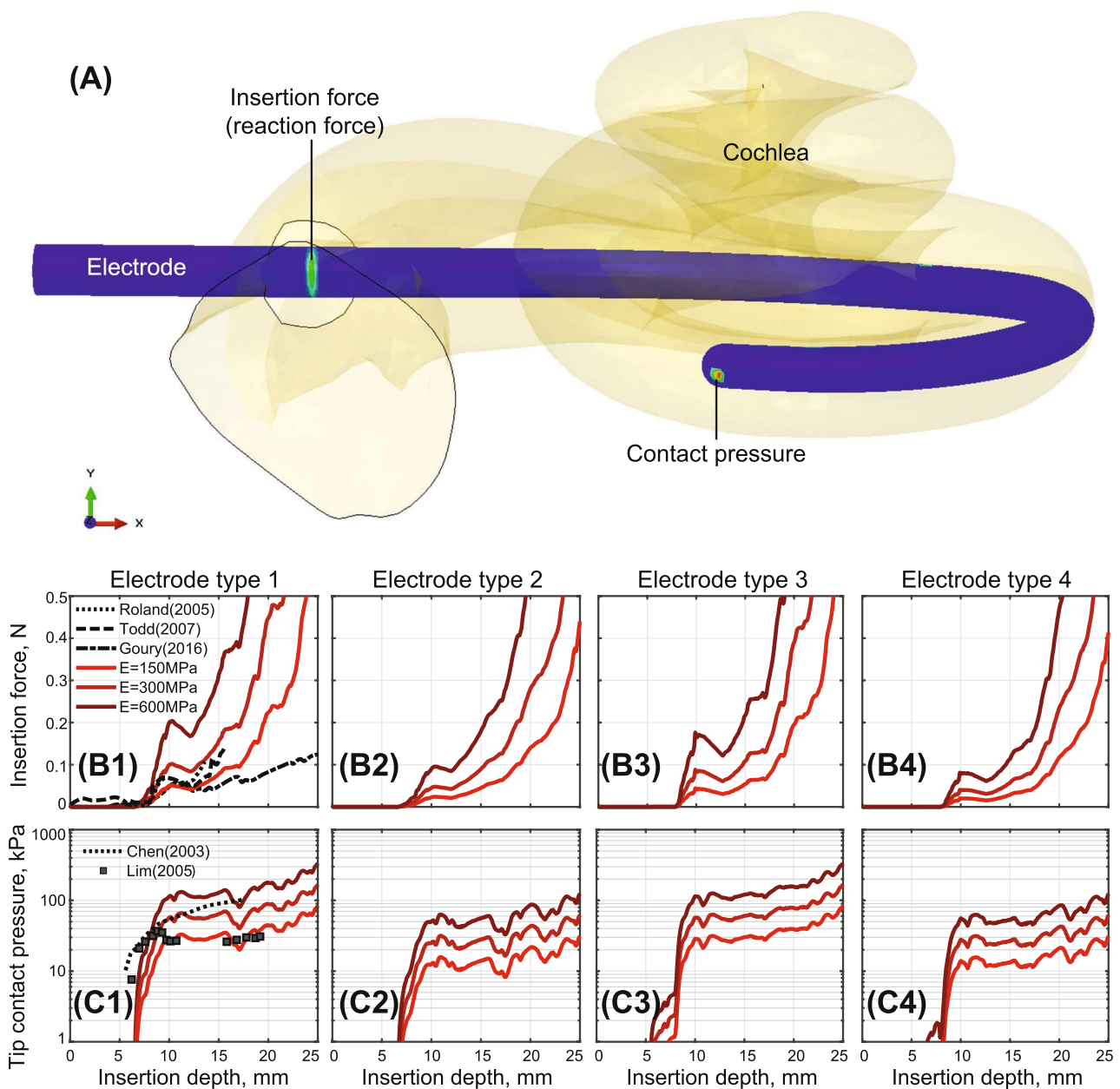
Fig. 4 The electrode insertion force and tip contact pressure. **A** A sketch for the obtainment of insertion force and tip contact pressure. **B1**–**B4** The insertion forces of four different electrode types; **C1**–**C4** The tip contact pressure of four different electrode types. For each electrode type, results of three different Young's modulus (150 MPa, 300 MPa, and 600 MPa) are plotted

the implantation of EA, which can be both experimentally measured or calculated through simulations (Roland 2005; Todd 2007; Goury et al. 2016). It is usually considered that higher insertion force adds difficulty in the insertion as well as the risk to harm the fragile structures within the cochlea. In this simulation, the insertion force is obtained from the electrode nodes that are nearing the center of the round window at each process. These nodes form a section that are inserted into the cochlea during the current time step, as shown in Fig. 4A. The insertion force is calculated as

the summation of x-directional reaction forces (which can be directly exported in Abaqus) associated with each node of this section. The tip contact pressure is defined as the nodal pressure between the electrode tip and the cochlear wall. At each insertion step, the maximum nodal pressure of the electrode nodes at the tip region (assumed as 0.25 mm length) was obtained.

Figure 4B1-B4 gives the insertion force curves from simulations of four types of EAs with three different Young's modulus, 100 MPa, 200 MPa and 400 MPa. Figure 4C1-C4
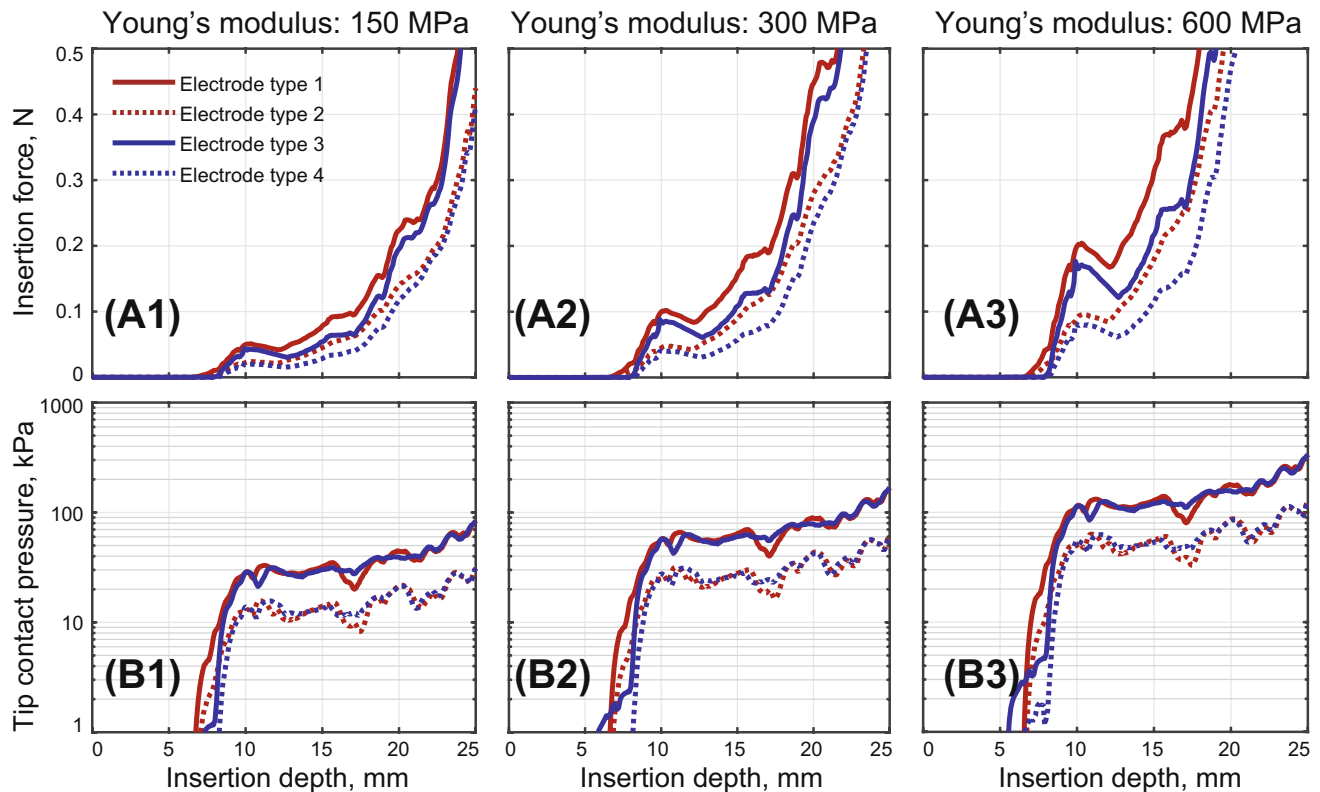
Fig. 5 Insertion force and tip contact pressure of different electrode types. **A1–A3** The insertion forces of four different electrode types, for three Young's modulus setups; **C1–C4** The tip contact pressure of four different electrode types. Red solid curve—electrode type 1 gives the corresponding contact pressure. In Fig. 4B1, previous experimental insertion force data by Roland (2005, in Fig. 12 - SIT) Roland (2005) and Todd (2007, in Fig. 2 - SIT) Todd (2007) and numerical results by Goury (2016, in Fig. 6 - successful insertion) Goury et al. (2016) were also plotted for comparison. In Fig. 4C1, the simulated contact pressure of Chen (2003, in Fig. 5 - design C), Chen et al. (2003) and Lim (2005, in Fig. 11 - profile 1) Lim et al. (2005) was plotted. Since the absolute values of contact pressure in literature vary from tens of kPa to several MPa, highly depending on the design of EA. Here, the data from Lim (2005) were scaled down by 0.1. All the data in literature were interpolated and smoothed for a better view, and the transition from the cochlear angle to the insertion depth were conducted whenever necessary.

The insertion force generally increases with the increase of the insertion depth (and the cochlear angle), and the forces are mostly within range of 0 to 0.5 N. Our results are consistent with previous data. The insertion force is near 0 before the EA touches the lateral wall of the cochlea (at cochlear angle about 150°, or insertion depth of about 8 mm), and increases nearly exponentially thereafter (Risi 2018). However, the profiles of the insertion force increase

(normal section size, straight); blue solid curve—electrode type 2 (tapered section size, straight); red dotted curve—electrode type 3 (normal section size, bended); and blue dotted curve - electrode type 4 (tapered section size, bended)

depends on factors such as the electrode model, the experimental measurement object (on plastic models or temporal bones), and the cochlear size. The profile of our simulated insertion force demonstrated a typical two-peak feature that has been reported by both Roland (2005); Todd (2007).

Similarly, both our simulation and the previous data show that the tip contact pressure has a dramatic increase after the electrode touch the intracochlear lateral wall (from insertion depth 6 to 8 mm), but the variation becomes smaller for further insertion.

3.2.1 Young's modulus

Comparing the curves representing different Young's modulus in each subplots of Fig. 4B1-B4 and C1-C4, it is obvious that the electrode Young's modulus is one of the dominating factors that influencing the EA insertion. Increasing the Young's modulus by a factor of 2 (from 150 MPa to 300 MPa, or from 300 MPa to 600 MPa), both the insertion force (B1-B4) and the tip contact pressure (C1-C4) are roughly doubled, indicating that they are proportional to the Young's modulus.

3.2.2 Different types of EA

Figure 5A1-A3 demonstrates the insertion forces of different electrode types, and Fig. 5B1-B3 gives the corresponding tip contact pressure. It is shown that the insertion force can be effectively reduced by tapering the EA section size, as well as making the EA pre-bended (see Fig. 5A1-A3). For example, the insertion force reaches 0.35 N for a normal-sized, straight EA, when implanted to 20 mm (red solid curve in Fig. 5A2), and reduced to 0.24 N when it is tapered (red dotted curve). When pre-bended, the insertion force reduced to 0.28 N (blue solid curve) and 0.18 N (blue dotted curve) for a normal and tapered EA. The insertion force is reduced by about 34% by tapering the EA, and by about 23% by pre-bending.

Similarly, tapering the EA would reduce the tip contact pressure by about 50% (see Fig. 5B1-B3). However, pre-bending the EA in this study has little effect on the tip contact pressure. The ineffectiveness of pre-bending on reducing tip contact force may be due to the relative straight shape of the pre-bended electrode tip (see Fig. 2).

3.3 Influence of insertion angle

Apart from the geometrical and mechanical properties of the EA, the insertion angle may also be crucial for a smooth implantation. In this study, we discussed four different angles, as shown in Fig. 6A. The insertion angle was defined as the angle formed by the EA and the centerline of the cochlea duct at the base (at about $\theta = 90°$). Four angles were analyzed, denoted as $-5, 0, +5, +10, +15$ degrees, where 0 degree is the "default" inserting angle (as shown in Fig. 1D), where the electrode was roughly parallel to the scala tympani centerline .

Figure 6B1-B4 presents the insertion force of the four EA types (all simulated with EA Young's modulus 300 MPa), influenced by different insertion angles. The insertion force increases with the insertion angle, for all simulated electrode types. But the maximum tip contact force is not significantly affected (see Fig. 6C1-C4).

3.4 Factors related with the EA insertion

3.4.1 The insertion force and intracochlear trauma

According to an indentation force measurement (Schuster et al. 2015), the rupture forces of the intracochlear soft structures were found between 42 and 122 mN, with a mean of 88 mN. Since the indentation force was applied perpendicularly to the basilar membrane, this force range is different from the insertion force during the EA implantation. De Seta (2017) reported an irregular, larger insertion force profile in the case of traumatic EA insertion, with an early peak force

of 30 ± 18.2 mN (De Seta et al. 2017), they conclude that the high peak force are correlated with basilar membrane lesion or translocation, with a high risk at 150° to 180°. However, another temporal bone study suggested that the basal trauma to the basilar membrane and osseous spiral lamina was related with the change in force profiles, but not necessarily the result of higher peak forces (Avci et al. 2017).

3.4.2 Design of the EA

To ensure a safe and smooth insertion, the geometrical and mechanical design of EA should be considered first (Dhanasingh and Jolly 2017). The EA stiffness is the most significant parameter. Reducing the EA stiffness would proportionally decreases the insertion force as well as the contact pressure, see Fig. 4. Although we adopted uniform effective Young's modulus to describe the EA stiffness, it was quite different from practical engineering. The EA stiffness is complicated, and determined by multiple factors, such as the number, the geometrical and material properties of metal wires, as well as their arrangement. Sometimes these factors may be optimized using intelligent algorithms. For example, Lim et al. (2005) found that with an optimized arrangement of metal wires, the tip contact pressure got minimal. In this arrangement, the wires roughly distributed vertically in the center in the EA, thus the bending modulus was minimal.

Another commonly used strategy is to soften the electrode tip, which can effectively reduce the insertion force and the contact pressure (Chen et al. 2003; Kha et al. 2007; Goury et al. 2016; Areias et al. 2021). Our simulations also show that tapering the EA would be beneficial (see Fig. 5).

The length of EA is another important parameter, which is not analyzed in this study. Currently the length of commercial EAs ranges from 14 mm to more than 30 mm. A longer EA, with deeper insertion, allows to stimulate lower-frequency regions of the cochlea, and to increase the performance of the CI. However, deeper insertion also indicate larger insertion force, thus increasing the risk of intracochlear trauma.

3.4.3 Other insertion choices or parameters

There are currently two surgical approaches: the cochleostomy (drilling an artificial hole near the round window), and the round window (enlarged if necessary) technique. Although the cochleostomy technique would be more smooth, it is still preferred to insert through the round window since it creates no extra trauma.

Simulations by Goury et al. (2016) indicated that a larger insertion angle would increase the insertion force, thus the force applied on the basilar membrane would increase accordingly. Aebischer et al. (2021) reported that insertion angles parallel to the scala tympani centerline would reduce
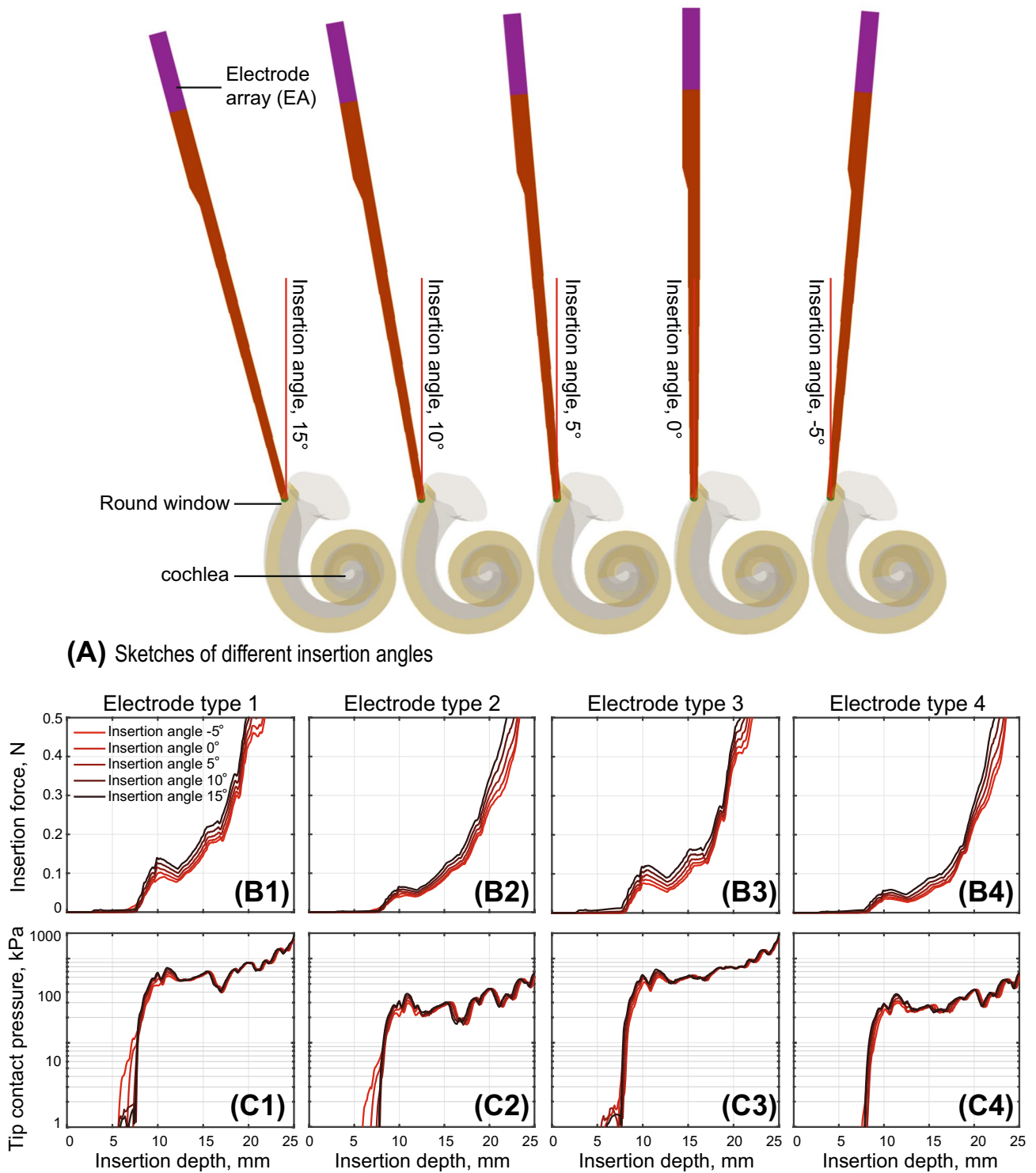
Fig. 6 The influence of insertion angle on the insertion force and tip contact pressure. **A** A sketch of four different insertion angles, namely, − 5, 0, + 5, + 10, + 15 degrees. **B1–B4** The insertion forces of four different electrode types; **C1–C4** The tip contact pressure of four different electrode types

the peak insertion forces (Aebischer et al. 2021). Our study also found that a smaller insertion angle would decrease the insertion force (e.g., −5° to 0° cases in Fig. 6).

The insertion speed has also been studied numerously. A low speed of insertion is beneficial to preservation of residual hearing (Kontorinis et al. 2011; Rajan et al. 2013) by reducing the insertion force. Using a 3D finite element model, Areias et al. (2021) simulated the influence of insertion speed (from 0.25 mm/s to 2 mm/s) on the insertion force, and the difference seems not very significant (Areias et al. 2021). Recently, it was found that using ultra-low insertion speed (<0.1 mm/s) would significantly reduce insertion force (Hügl et al. 2018, Zuniga et al. 2021). When the insertion speed is sufficient slow, the insertion force would converge to minimum. That is one reason that we used the quasi-static analysis.

3.5 Limitations and future work

The first limitation of the current work is the homogenous simplification of the EA, whereas in practical the EA is really complicated, made of thin platinum wires, contact metal electrodes embedded in a silicone base. The arrangement of these tiny metal structures should have great influence on the mechanical properties, and a homogenous assumption of EA is indeed over-simplified. Therefore, experimental verifications are necessary for evaluate the accuracy of this finite element framework, which should be our future work in priority.

Another limitation of this paper is that we adopted an average SSM model for the cochlea, but insertion dynamics (force profiles, contact pressure, etc.) the patient-specific cochlear geometry may be different. Therefore, one of our next work is to study the influence of cochlear geometrical parameters (such as its length or section size).

4 Conclusions

In this study, we developed a finite element framework to study the quasi-dynamic EA insertion process during CI surgery. The EA design parameters (Young's modulus, different types of EA design), the insertion angle, and the cochlear geometrical alterations were discussed based on the insertion force and tip contact pressure. We found (1) the EA stiffness is the most important design factor to reduce the insertion force; (2) tapering and pre-bending are effectively in reducing force-induced intracochlear trauma; (3) Aligning the insertion angle to the centerline of the basal scala tympani gives positive influence on smooth insertion. This framework is proven to be an useful tool for optimizing EA

designs, and is potentially benefficence for designing patient-specific CI surgery.

Author contributions **LJR** contributed to methodology, conceptualization, software, visualization, and writing—original draft. **YY** contributed to methodology, visualization, software, formal analysis, and writing—review and editing. **YHZ** contributed to resources, methodology, and writing—review and editing. **XDL, ZJS** contributed to resources and methodology **WJY** contributed to writing—review and editing and funding. **TYZ** contributed to writing—review and editing and funding. **CW** contributed to resources, conceptualization, and writing—review and editing. **CLL** contributed to conceptualization and writing—review and editing. All authors contributed to the article and approved the submitted version.

Declarations

Conflict of interest The authors declares no conflict of interest for this work.

References

AB Grayeli, C Guigou, and G Leterme (2014) Minimally invasive cochlear implantation: Anatomical and technical considerations. *COCHLEAR IMPLANTS*, p 49

AN Vadivelu, Z Liu, DS Gunawardena, B Chen, H-Y Tam, S O'Leary, and D Oetomo (2019) Integrated force sensor in a cochlear implant for hearing preservation surgery. In: 2019 41st annual international conference of the IEEE engineering in medicine and biology society (EMBC), pp 3819–3822s. IEEE

Aebischer P, Mantokoudis G, Weder S, Anschuetz L, Caversaccio M, Wimmer W (2021) In-vitro study of speed and alignment angle in cochlear implant electrode array insertions. IEEE Trans Biomed Eng 69(1):129–137

Areias B, Parente MPL, Gentil F, Natal Jorge RM (2021) Finite element modelling of the surgical procedure for placement of a straight electrode array: Mechanical and clinical consequences. J Biomech 129:110812

Avci E, Nauwelaers T, Hamacher V, Kral A (2017) Three-dimensional force profile during cochlear implantation depends on individual geometry and insertion trauma. Ear Hear 38(3):e168–e179

Caversaccio M, Gavaghan K, Wimmer W, Williamson T, Ansò J, Mantokoudis G, Gerber N, Rathgeb C, Feldmann A, Wagner F et al (2017) Robotic cochlear implantation: surgical procedure and first clinical experience. Acta Otolaryngol 137(4):447–454

Chen BK, Clark GM, Jones R (2003) Evaluation of trajectories and contact pressures for the straight nucleus cochlear implant electrode array-a two-dimensional application of finite element analysis. Med Eng Phys 25(2):141–147

De Seta D, Torres R, Russo FY, Ferrary E, Kazmitcheff G, Heymann D, Amiaud J, Sterkers O, Bernardeschi D, Nguyen Y (2017) Damage to inner ear structure during cochlear implantation: correlation

between insertion force and radio-histological findings in temporal bone specimens. Hearing Res 344:90–97

De Seta D, Daoudi H, Torres R, Ferrary E, Sterkers O and Nguyen Y (2021) Robotics, automation, active electrode arrays, and new devices for cochlear implantation: a contemporary review. *Hearing Res*, p 108425

Dhanasingh A, Jolly C (2017) An overview of cochlear implant electrode array designs. Hear Res 356:93–103

Fayad JN, Makarem AO, Linthicum FH Jr (2009) Histopathologic assessment of fibrosis and new bone formation in implanted human temporal bones using 3d reconstruction. Otolaryngol-Head Neck Surg 141(2):247–252

Gerber N, Reyes M, Barazzetti L, Kjer HM, Vera S, Stauber M, Mistrik P, Ceresa M, Mangado N, Wimmer W et al (2017) A multiscale imaging and modelling dataset of the human inner ear. Sci Data 4(1):1–12

Holden LK, Finley CC, Firszt J, Holden T, Brenner C, Potts LG, Gotter BD, Vanderhoof SS, Mispagel K, Heydebrand G et al (2013) Factors affecting open-set word recognition in adults with cochlear implants. Ear Hearing 34(3):342

Hügl S, Rülander K, Lenarz T, Majdani O, Rau TS (2018) Investigation of ultra-low insertion speeds in an inelastic artificial cochlear model using custom-made cochlear implant electrodes. Eur Arch Oto-Rhino-Laryngology 275(12):2947–2956

Jin Xu, Shi-Ang Xu, Cohen Lawrence T, Clark Graeme M (2000) Cochlear view: postoperative radiography for cochlear implantation. Otology Neurotol 21(1):49–56

Kalkman RK, Briaire JJ, Frijns JHM (2016) Stimulation strategies and electrode design in computational models of the electrically stimulated cochlea: An overview of existing literature. Network Comput Neural Syst 27(2–3):107–134

Kamakura T, Nadol JB Jr (2016) Correlation between word recognition score and intracochlear new bone and fibrous tissue after cochlear implantation in the human. Hearing Res 339:132–141

Kha HN, Chen BK (2006) Determination of frictional conditions between electrode array and endosteum lining for use in cochlear implant models. J Biomech 39(9):1752–1756

Kha H, Chen B (2012) Finite element analysis of damage by cochlear implant electrode array's proximal section to the basilar membrane. Otology Neurotol 33(7):1176–1180

Kha HN, Chen BK, Clark GM (2007) 3d finite element analyses of insertion of the nucleus standard straight and the contour electrode arrays into the human cochlea. J Biomech 40(12):2796–2805

Kha HN, Chen BK, Clark GM, Jones R (2004) Stiffness properties for nucleus standard straight and contour electrode arrays. Med Eng Phys 26(8):677–685

Kobler J-P, Beckmann D, Rau TS, Majdani O, Ortmaier T (2014) An automated insertion tool for cochlear implants with integrated force sensing capability. Int J Comput Assisted Radiol Surg 9(3):481–494

Kontorinis G, Lenarz T, Stöver T, Paasche G (2011) Impact of the insertion speed of cochlear implant electrodes on the insertion forces. Otology Neurotol 32(4):565–570

Kratchman LB, Schuster D, Dietrich MS, Labadie RF (2016) Force perception thresholds in cochlear implantation surgery. Audiol Neurotol 21(4):244–249

Lim YS, Park S-I, Kim YH, Oh SH, Kim SJ (2005) Three-dimensional analysis of electrode behavior in a human cochlear model. Med Eng Phys 27(8):695–703

Majdani O, Rau TS, Baron S, Eilers H, Baier C, Heimann B, Ortmaier T, Bartling S, Lenarz T, Leinung M (2009) A robot-guided minimally invasive approach for cochlear implant surgery: preliminary results of a temporal bone study. Int J Comput Assisted Radiol Surg 4(5):475–486

N Duchateau, N Mangado, M Ceresa, P Mistrik, S Vera, and MAG Ballester (2015) Virtual cochlear electrode insertion via parallel transport frame. In: 2015 IEEE 12th International symposium on biomedical imaging (ISBI), pp 1398–1401. IEEE

O Goury, Y Nguyen, R Torres, J Dequidt, and C Duriez (2016) Numerical simulation of cochlear-implant surgery: towards patient-specific planning. In: International conference on medical image computing and computer-assisted intervention, Springer, pp 500–507

Rajan GP, Kontorinis G, Kuthubutheen J (2013) The effects of insertion speed on inner ear function during cochlear implantation: a comparison study. Audiol Neurotol 18(1):17–22

Riojas KE, Labadie RF (2020) Robotic ear surgery. Otolaryngol Clin North Am 53(6):1065–1075

Risi F (2018) Considerations and rationale for cochlear implant electrode design-past, present and future. J Int Adv Otology 14(3):382

Roland JT Jr (2005) A model for cochlear implant electrode insertion and force evaluation: results with a new electrode design and insertion technique. The Laryngoscope 115(8):1325–1339

Roland PS, Wright CG (2006) Surgical aspects of cochlear implantation: mechanisms of insertional trauma. Cochlear Brainstem Implants 64:11–30

Sato H, Sando I, Takahashi H (1991) Sexual dimorphism and development of the human cochlea: computer 3-d measurement. Acta Otolaryngol 111(6):1037–1040

Schuster D, Kratchman LB, Labadie RF (2015) Characterization of intracochlear rupture forces in fresh human cadaveric cochleae. Otology Neurotol: Official Publication Am Otological Soc, Am Neurotol Soc Eur Acad Otology Neurotol 36(4):657

ThS Rau A, Hussong M Leinung, Lenarz T, Majdani O (2010) Automated insertion of preformed cochlear implant electrodes: evaluation of curling behaviour and insertion forces on an artificial cochlear model. Int J Comput Assisted Radiol Surg 5(2):173–181

Thong JF, Low D, Tham A, Liew C, Tan TY, Yuen HW (2017) Cochlear duct length-one size fits all? Am J Otolaryngol 38(2):218–221

Todd CA, Naghdy F (2012) Haptic modelling of cochlear implantation. Int J Biomed Eng Technol 8(4):375–394

Todd CA, Naghdy F, Svehla MJ (2007) Force application during cochlear implant insertion: an analysis for improvement of surgeon technique. IEEE Trans Biomed Eng 54(7):1247–1255

Wade SA, Fallon JB, Wise AK, Shepherd RK, James NL, Stoddart PR (2014) Measurement of forces at the tip of a cochlear implant during insertion. IEEE Trans Biomed Eng 61(4):1177–1186

Zeng F-G, Rebscher S, Harrison W, Sun X, Feng H (2008) Cochlear implants: system design, integration, and evaluation. IEEE Rev Biomed Eng 1:115–142

Zuniga MG, Hügl S, Engst BG, Lenarz T, Rau TS (2021) The effect of ultra-slow velocities oninsertion forces: A study using a highly flexible straight electrode array. Otol Neurotol 42(8):1013–1021